Indian Journal of Chemistry
Vol. 56A, October 2017, pp. 1041-1047

Notes

Structural and magnetic characterization of nanocrystalline $LaFeO_3$ synthesized by low temperature combustion technique using different fuels

Suram Singh & Devinder Singh*

Department of Chemistry, University of Jammu, Jammu 180 006, India

Email: drdssambyal@rediffmail.com

Synthesis of nanocrystalline $LaFeO_3$ with fine particle size by a simple combustion method employing urea and polyvinyl alcohol as combustion fuels without using water or any other solvent is reported. Rietveld structural refinement analysis of the powder X-ray diffraction data indicates that $LaFeO_3$ crystallizes in the orthorhombic perovskite structure with space group *Pbnm*. The values of unit cell volume and X-ray density of the samples remain almost constant, indicating the efficiency of the combustion method. The average grain size of $LaFeO_3$ powders obtained with urea as a fuel is smaller, while the specific surface area is larger than that of the nanopowder obtained with polyvinyl alcohol. Both the phases show antiferromagnetic behavior and antiferromagnetic interactions are dominant in the phase synthesized by polyvinyl alcohol. Anti-ferromagnetic behavior of the samples may be due to super-exchange Fe^{3+}–O^{2-}–Fe^{3+} interactions.

Keywords: Nanomaterials, Perovskites, Orthoferrites, Oxides, Antiferromagnetic properties, Combustion method, Magnetic properties, Iron oxide, Lanthanum, Urea, Polyvinyl alcohol

Over the past few years, the fabrication and characterization of nanosized or submicroscopic materials hold a great promise as the materials in this size range would be technologically important because of their size dependent novel properties to meet stringent requirements in new potential applications. Orthoferrites ($RFeO_3$, R = rare earth elements) belonging to this important class of materials are gaining prominence owing to their unique and fruitful properties and thus have attracted the attention of many scientists and researchers.[1-5]

$LaFeO_3$ is an antiferromagnetic insulator with a Néel temperature of ~450°C.[4,6] It crystallizes in the orthorhombic perovskite structure at room temperature and undergoes a phase transition to the rhombohedral symmetry at about 987 °C.[7] The magnetic properties of $LaFeO_3$ have been extensively studied for the past many years but those of $LaFeO_3$ nanoparticles are rare.[8] Antiferromagnetic (AFM) nanoparticles always show unusual magnetic properties due to the finite size and surface anisotropy effects.[9-11] The decrease in particle size of $LaFeO_3$ has been expected to improve the magnetic property.[12] The ferromagnetism (FM) in $LaFeO_3$ with particle size of ~10–50 nm has been reported due to the presence of uncompensated surface spin, which is called the FM shell, surrounding the AFM core of the nanoparticles.[13-15]

Several soft-chemical approaches such as sol-gel, co-precipitation, citrate-gel and combustion methods yield nanosized particles with good homogeneity, low porosity and good control over particle size.[16-20] Among these soft-chemical methods, the combustion synthesis exhibits many advantages and has been used for the large scale production of nanoparticles with high surface area. This method of synthesis is advantageous due to its simplicity, short amount of time and lower consumption of energy during synthesis.[21-23] Further, the combustion reaction mainly depends upon the choice of fuel and the oxidizer-to-fuel ratio, since it liberates maximum amount of heat energy based on the reducing power of the fuel.[24]

Although there are numerous reports for preparing $LaFeO_3$ nanopowders by combustion methods in liquid media, to the best of our knowledge, $LaFeO_3$ nanopowders, prepared by combustion process without using water in order to completely avoid impurities caused by water, has not been reported in the literature. In our previous work,[25] we have synthesized $LaFeO_3$ nanopowders successfully by glycine-nitrate combustion method without using water to obtained the precursor. In order to see the effect of other fuels on structural and magnetic properties of $LaFeO_3$, we report here the synthesis of nanocrystalline $LaFeO_3$ powders by low temperature combustion method using fuels like urea and polyvinyl alcohol (PVA) and investigate the influence of fuels on the particle size control, structural aspects and magnetic properties of $LaFeO_3$ nanopowders.

Experimental

Nanocrystalline powders of $LaFeO_3$ were prepared by the combustion reaction technique using urea and polyvinyl alcohol (PVA) as the combustion fuels.

AR grade lanthanum nitrate, $La(NO_3)_3.6H_2O$ (Loba Chemicals, 99.9%), iron nitrate, $Fe(NO_3)_3.9H_2O$ (Loba Chemicals, 99.9%), polyvinyl alcohol, $[(-C_2H_4O)_n]$ (Loba Chemicals, 99%), and urea (NH_2CONH_2) (Loba Chemicals, 99.5%) were used as starting materials. The combustion ratio of oxidizer (O) and fuel (F), i.e., Φ_e (O/F), was calculated using the total valence of oxidizers (metal nitrates) and the reducing valence of the fuels (urea, PVA) according to the principle of propellant chemistry.[24] The value Φ_e was taken as unity as it serves as the maximum heat release at the time of combustion. The number of moles of fuels involved in the stoichiometry of the redox mixture for combustion were calculated by the methods described elsewhere.[25,26] Therefore, the composition of reaction mixture requires 5 moles of urea and 3 moles of PVA for the synthesis of 1 mole of $LaFeO_3$ as shown in balanced combustion reactions.

The stoichiometric amounts of metal nitrates were mixed together thoroughly in an agate mortar and pestle to get a homogeneous mixture. After that, urea/ PVA in the required molar ratio were added to the mixture as a chelator and as a fuel without adding water. The slurry was formed due to the hygroscopic nature of metal nitrates. In the combustion process, firstly the slurry undergoes dehydration at 80 °C followed by spontaneous combustion at 250 °C with the evolution of voluminous gases yielding a voluminous and foamy product. The entire combustion reaction was completed within few minutes. The foamy powder was then calcined in static air at 500 °C for 2 h in the muffle furnace to obtain the fine powder of $LaFeO_3$. An interesting feature of the present method is that it does not require water or any other solvent to obtain the precursor and therefore, avoids impurities caused by water completely. The samples obtained by using urea and PVA as fuel were named as U and P respectively.

The possible chemical reactions for the synthesis of U and P phases can be represented by the following equations;

$$La(NO_3)_3.6H_2O + Fe(NO_3)_3.9H_2O + 5NH_2CONH_2 \rightarrow LaFeO_3 + 5CO_2\uparrow + 25H_2O\uparrow + 8N_2\uparrow$$

$$La(NO_3)_3.6H_2O + Fe(NO_3)_3.9H_2O + 3C_2H_4O \rightarrow LaFeO_3 + 6CO_2\uparrow + 21H_2O\uparrow + 3N_2\uparrow$$

The phase constitution of the obtained products was characterized by using PANanalytical X'PertPRO MRD, Netherlands, equipped with Ni-filtered CuKα radiations operated at 45 kV and 40 mA. XRD measurements were taken at room temperature in the 2θ scanning range from 20° to100° with a step size of 0.0171° and continuous scan step time of 21 s. The structural parameters were determined for each sample by the Rietveld structural refinement method using the GSAS software.[27] The average crystallite sizes were calculated using XRD data, employing Debye-Scherrer's formula.[28] The densities of the sintered samples were determined by Archimedes method. The microstructures of the products were examined by scanning electron microscope FE-SEM Quanta 200 FEG with an accelerating voltage of 200V–30 kV. Energy-dispersive X-ray analysis (EDS) spectra were measured on a JEOL-JSM-840 scanning microscope using INCA attachment with the SEM instrument. The particle size of the nanopowders was determined by transmission electron microscope (TEM, model Technai G2 20 S-TWIN FEI Netherlands). Samples for TEM analysis were prepared by placing a drop of the powder sample suspension after treated with oscillation thoroughly on a carbon-coated copper TEM grid, allowing it to dry in air and analyzed at an accelerating voltage of 20–200 kV. The magnetization versus temperature measurements of as-prepared samples were recorded within the temperature range 80-300 K and a static applied magnetic field of 0.4 T using Faraday magnetic balance, provided with Polytronic made electromagnet.

Results and discussion

The XRD patterns of the obtained $LaFeO_3$ nanopowders show a high degree of crystallinity as indicated by the appearance of intense reflections (Fig. 1). The diffraction peaks of these powders could be indexed to an orthorhombic structure with the space group *Pbnm*. The structural parameters were refined by the Rietveld method using the GSAS software. The structure refinement was performed in the orthorhombic setting of the *Pbnm* space group, with La at 4c(*x*, *y*, 0.25), Fe at 4b(0, 0.5, 0), O(1) at 4c(*x*, *y*, 0.25) and O(2) at 8d(*x*, *y*, *z*).

A sixth-order Chebychev polynomial for the background, zero, LP factor, scale, pseudo-Voigt profile function (*U*, *V*, *W* and *X*), lattice parameters, atomic coordinates and isothermal temperature factors U_{iso} were used in the refinement. Isotropic thermal displacement parameters, initially set at 0.025 $Å^2$, were refined first for the metal atoms and then for the

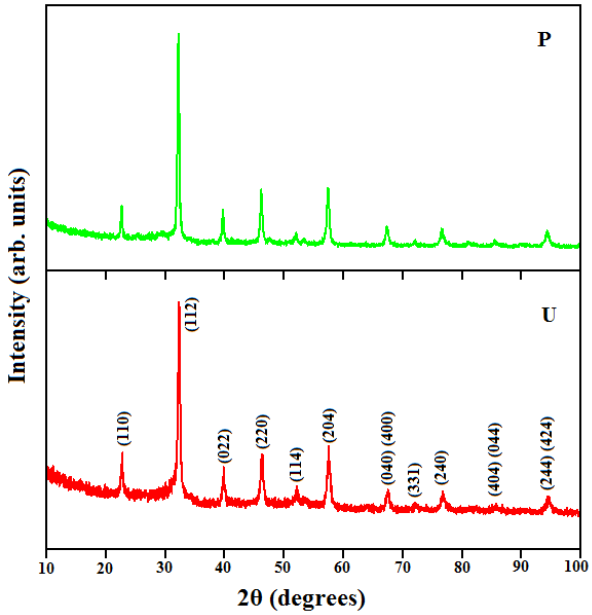

Fig. 1 – Powder X-ray diffraction patterns of nanocrystalline $LaFeO_3$ powders.

Table 1 – Structural parameters obtained from the Rietveld refinement of XRD patterns for $LaFeO_3$ samples calcined at 500 ºC. [The atomic sites are: La 4c[*x*, *y*, 0.25]; Fe 4b[0, 0.5, 0]; O(1) 4c[*x*, *y*, 0.25]; O(2) 8d[*x*, *y*, *z*] in the space group *Pbnm*]

Parameter		U	P
a (Å)		5.5700(20)	5.5576(15)
b (Å)		5.5490(16)	5.5538(14)
c (Å)		7.8260(17)	7.8383(11)
V (Å^3)		241.89(12)	241.94(10)
x	La	-0.0046(10)	-0.0035(5)
	O(1)	0.005(8)	0.062(4)
	O(2)	0.6712(27)	0.7311(18)
y	La	0.0232(10)	0.0244(5)
	O(1)	0.426(8)	0.483(4)
	O(2)	0.2270(27)	0.2869(18)
z	O(2)	-0.0157(27)	0.0442(18)
U_{iso} (Å^2)	La	0.02305(8)	0.02176(6)
	Fe	0.02636(5)	0.01515(8)
	O(1)	0.08073(4)	0.08202(7)
	O(2)	0.02500(6)	0.03314(4)
R_{wp}		0.1662	0.1324
R_p		0.1250	0.0983
χ^2		2.030	1.294

oxygen atoms with full occupancy. The occupation factors for the metals were fixed by taking sample stoichiometry into account, while those of oxygen atoms were refined. No evidence of oxygen non-stoichiometry could be obtained from the XRD structural refinements and the oxide ion sites were therefore fixed at full occupancy. There is good

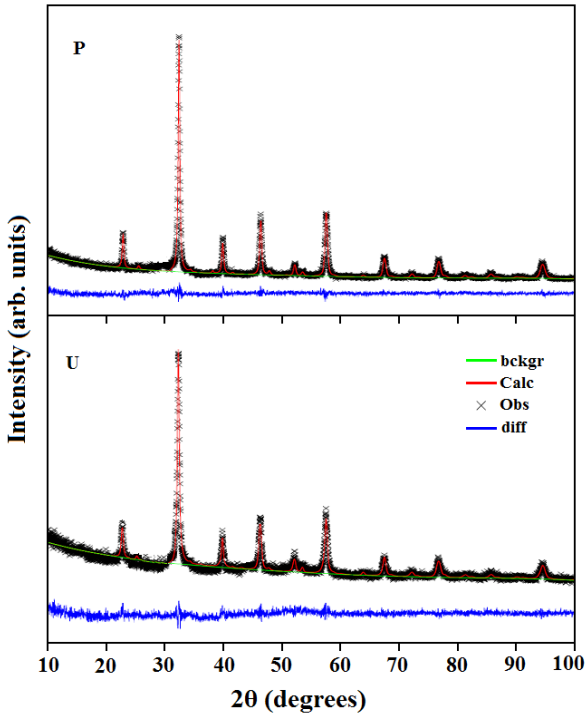

Fig. 2 – Rietveld refinement of X-ray diffraction data for $LaFeO_3$ powders.

agreement between observed and calculated patterns as shown in Fig. 2. The refined structural parameters along with the residuals for the weighted pattern R_{wp}, the pattern R_p, and the goodness of fit χ^2 of the samples are summarized in Table 1. The obtained lattice parameters of both the samples were in good agreement with those reported previously.[4] It can be seen that there is almost no change in the values of unit cell volume and X-ray density of the two samples indicating efficiency of combustion methods for preparation of $LaFeO_3$ nanoparticles (Table 1). The slightly larger unit cell volume and lower density of sample P may be due to its larger crystallite size.

For the combustion synthesis, the crystallite size and the extent of the agglomeration of products are generally affected by the speed and temperature of the combustion reaction, which are dependent on the nature of the fuel.[29] Our results show that the crystallite size of sample U (20 nm) is smaller than that of P (28 nm) due to its low decomposition temperature for combustion reaction and the large amount of gases evolved, which enhances the dissipation of heat and limits the inter-particle contact.[30]

The percentage porosity of the samples was calculated using the relationship[31],

$P = \left[1 - \left(\frac{d_{\exp}}{d_{XRD}}\right)\right] \times 100$ where d_{exp} is the measured density and d_{XRD} is the X-ray density. The X-ray density was found to be 6.666 g cm^{-3} and 6.664 g cm^{-3} for U and P respectively, while the percentage porosity was 6.8 and 9.8 respectively for U and P. The larger bulk density (d_{exp}) of sample U (6.212 g cm^{-3}) as compared to that of P (6.012 g cm^{-3}) could be due to smaller crystallite size of the former.

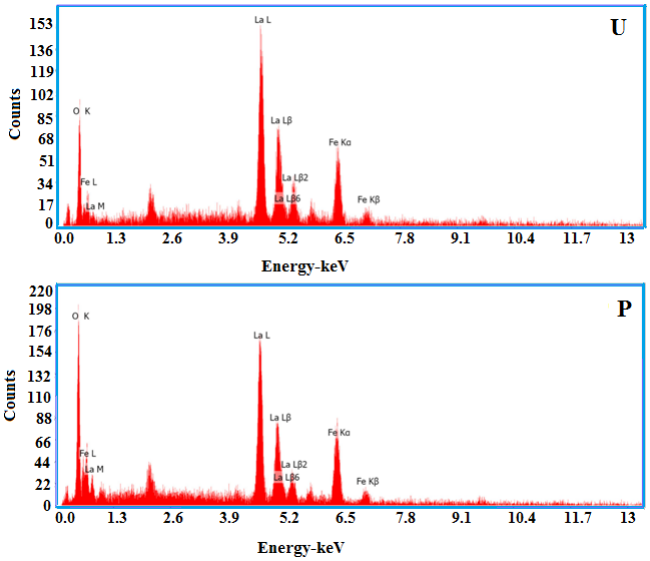

Fig. 3 – EDX spectra of nanocrystalline $LaFeO_3$ samples.

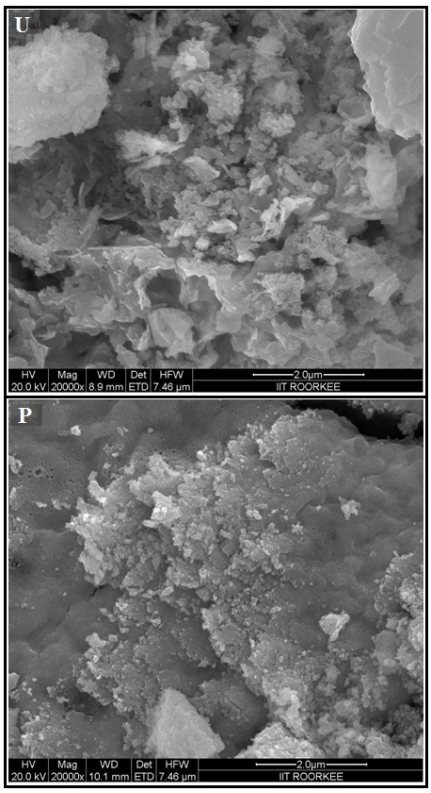

Fig. 4 – SEM micrographs showing the morphology of nanocrystalline $LaFeO_3$ powders.

The composition of $LaFeO_3$ nanopowders was determined by energy dispersive X-ray analysis (EDX) (Fig. 3). The EDX results confirm the presence of elements, La, Fe, and O, in the samples. The analysis was done on three different regions. A typical cationic composition has been calculated from the averages of mass percentage of these three regions. The experimental mass for La was found to be 56.91% and 57.13% respectively in U and P (theoret. 57.22%). The respective values for Fe was 23.29% and 23.40% (theoret. 23.00%), while for O these values were 19.80% and 19.47% (Theoret. 19.77%). Elemental analysis (mass%) of La, Fe and O calculated from EDX spectrum and the theoretical values are in good agreement.

Figure 4 shows the typical SEM micrographs of the $LaFeO_3$ powders. It is clearly seen that the sample U had highly porous networks with voids and holes contribute to amorphous-like features which could be attributed to the escaping of large amount of gases during combustion reactions while in case of sample P, SEM micrograph reflects a well crystalline formation of $LaFeO_3$ powder consisting of highly agglomerated particles a part of which become sponge-like form.[32] However, the grain boundaries in both the samples are completely invisible. In fact, the formation of such objects is typical of combustion synthesis, which depends upon the choice of fuel and the oxidizer to fuel ratio, since it liberates maximum amount of heat energy based on the reducing power of the fuel.[24]

Representative TEM images of U and P samples clearly show that particles of both the nanopowders, U and P, are homogenous, well dispersed and possess spherical symmetry with the average particle size between 30 and 42 nm (Fig. 5). This additional evidence confirms that the small particles obtained by this combustion method are indeed nanometer in dimension. The particle sizes observed by TEM are larger than those of crystallite sizes calculated by XRD, which indicates that each particle observed by TEM consists of several crystallized grains.[33] This may be due to the presence of non-crystalline surface layers, resulting in increase in the particle size which is not determined by XRD.[34]

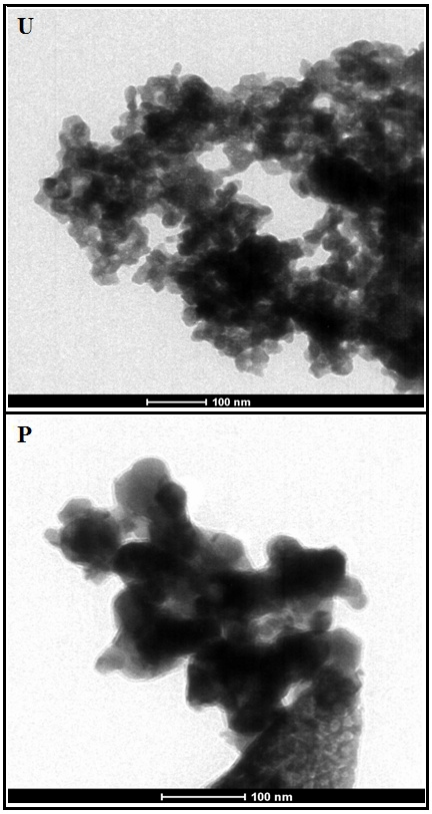

Fig. 5 – TEM micrographs of nanocrystalline $LaFeO_3$ powders.

The specific surface area (S) for the as-prepared samples can be calculated using the equation[35], $S = 6000/ d.D_{XRD}$, where d is density and D_{XRD} is the crystallite size obtained from XRD in nm. The values of surface area were calculated by using both X-ray (44.2 and 32.0 m^2 g^{-1} for U and P respectively) and bulk density (48.3 and 35.6 m^2 g^{-1} for U and P respectively). The specific surface area of powder U was found to be larger than that of sample P. The more disordered porous structure in the particles and the relative small particle size of nanopowder U are responsible for its high surface area.

The temperature dependence of the molar magnetic susceptibility for nanocrystalline $LaFeO_3$ samples is shown in Fig. 6. The results indicate that magnetization of U sample is lower than that of sample P. The magnetic behavior of the nanocrystalline powders is mainly explained by surface effects where fewer magnetic moments are participating due to the less perfect crystalline structure.[36,37] Therefore, it is concluded that less crystallinity of sample U could lead to its smaller magnetization.

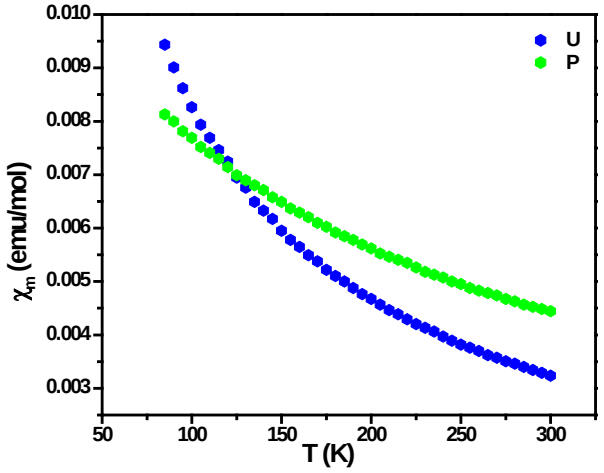

Fig. 6 – Plots of molar magnetic susceptibility as a function of temperature for nanocrystalline $LaFeO_3$ powders.

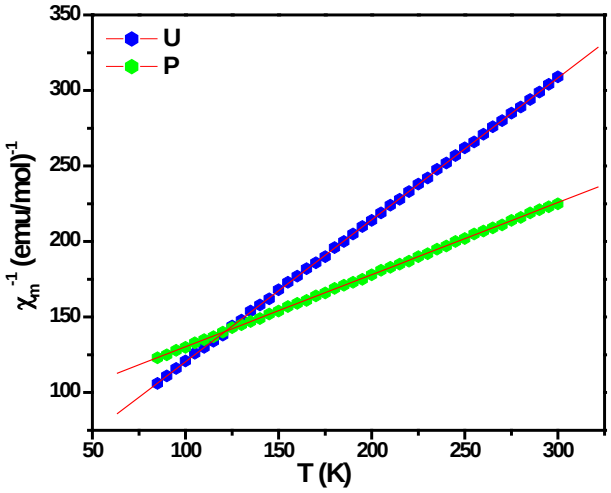

Fig. 7 – Plots of inverse molar magnetic susceptibility versus temperature of nanocrystalline $LaFeO_3$ powders.

Both the samples obey Curie-Weiss law and the plots are shown in Fig. 7. Fitting of the experimental inverse magnetic susceptibility versus temperature pattern over the whole temperature range studied from 80-300 K by Curie-Weiss law ($\chi = C/T - \theta$) yields the Curie and Weiss constants C and Θ. The Weiss constant (Θ) is determined from the curve by extrapolating the straight line towards the temperature axis, as shown in Fig. 7. The slope of the curve determines the value of Curie constant (C) which is defined as; $C = N_A \mu_B^2 \mu_{eff}^2 / 3k_B$, where N_A (= 6.023×10^{23} mol^{-1}) is the Avogadro number; μ_B (= 9.274×10^{-21} emu) is the Bohr magneton; μ_{eff} is the observed effective moment expressed in Bohr

magneton and k_B (= 1.38016×10^{-16} erg K^{-1}) is the Boltzmann constant.

The Weiss constant (Θ) is negative for both the samples indicating the presence of anti-ferromagnetic interactions (–28 and –172 for U and P respectively). The anti-ferromagnetic behavior could be due to the presence of superexchange Fe^{3+}–O–Fe^{3+} interactions.[38-40] The experimental effective paramagnetic moments (μ_{eff}) was calculated from the relation: $\mu_{eff} = 2.828\sqrt{C}$. The theoretical spin only moment (5.91 B M) can be calulated as; $\mu_S = g\sqrt{S(S+1)}$ where g (= 2) is the gyromagnetic factor and S (= 5/2) is the spin of the Fe^{3+} cation. The μ_{eff} values of both the samples (2.91 BM and 4.08 BM for U and P respectively) were found to be smaller than spin only magnetic moment of Fe^{3+} (5.91 BM), which may be attributed to the presence of anti-ferromagnetic interactions. The smaller effective magnetic moment and lesser negative value of Θ of the nanopowder U indicate that fewer magnetic moments are participating due to its less perfect crystalline structure.[36,37]

In the current study, $LaFeO_3$ powders have been synthesized with shorter calcining times and low temperature combustion method using different fuels. Rietveld refinements show that the synthesized powders are nanocrystalline materials with high purity and good homogeneity which crystallize with orthorhombic unit cell in the space group *Pbnm*. The phase formation, crystallite size and specific surface area are strongly dependent on the nature of the fuel. The sample U has smaller crystallite size and hence larger specific surface area than that of sample P because of low decomposition temperature of urea for combustion. Grain size obtained from TEM studies is found to be larger than that crystallite size obtained from XRD in both the samples. The Weiss constant (Θ) is negative for the nanopowders, indicating the presence of antiferromagnetic interactions. The smaller molar magnetic susceptibility and effective magnetic moment of the nanopowder U than that of sample P indicate that fewer magnetic moments are participating due to the less perfect crystalline structure of the former.

Acknowledgement

We are thankful to University Grants Commission, New Delhi (India) for financial support under the Rajiv Gandhi National Fellowship (RGNF) funded by UGC (Grant No. F. 14-2(ST)/2010 (SA-III) dated: May, 2011). We are also thankful to Dr. Harpreet Singh, Central Research Facility Section, Indian Institute of Technology Ropar, India, for recording XRD. Thanks are also due to Prof. Ramesh Chandra, Institute Instrumentation Centre, Indian Institute of Technology, Roorkee, India, for recording EDX, SEM and TEM.

References

1 Ding J, Lü X, Shu H, Xie J & Zhang H, *Mater Sci Eng B*, 171 (2010) 31.
2 Sivakumar M, Gedanken A, Bhattacharya D, Brukental I, Yeshurun Y, Zhong W, Du YW, Felner I & Nowik I, *Chem Mater*, 16 (2004) 3623.
3 Wu A H, Shen H, Xu J, Jiang L W, Luo L Q, Yuan S J, Cao S X & Zhang H J, *J Sol-Gel Sci Technol*, 59 (2011) 158.
4 Cristóbal A A, Botta P M, Aglietti E F, Conconi M S, Bercoff P G & Porto López J M, *Mater Chem Phys*, 130 (2011) 1275.
5 Wang D, Chu X F & Gong M L, *Nanotechnology*, 17 (2006) 5501.
6 Seo J W, Fullerton E E, Nolting F, Scholl A, Fompeyrine J & Locquet J -P, *J Phys Condens Matter*, 20 (2008) 264014.
7 Geller S & Raccah P M, *Phys Rev B*, 2 (1970) 1167.
8 Rajendran M & Bhattacharya A K, *J Eur Ceram Soc*, 26 (2006) 3675.
9 Kodama R H, Makhlouf S A & Berkowitz A E, *Phys Rev Lett*, 79 (1997) 1393.
10 Winkler E, Zysler R D, Mansilla M V & Fiorani D, *Phys Rev B*, 72 (2005) 132409.
11 Kodama R H & Berkowitz A E, *Phys Rev B*, 59 (1999) 6321.
12 Phokha S, Pinitsoontorn S, Maensiri S & Rujirawat S, *J Sol-Gel Sci Technol*, 71 (2014) 333.
13 Saad A A, Khan W, Dhiman P, Naqvi A H & Singh M, *Electron Mater Lett*, 9 (2013) 77.
14 Thuy N T & Minh D L, *Adv Mater Sci Eng*, (2012) doi:10.1155/2012/380306.
15 Lee W Y, Yun H J & Yoon J W, *J Alloys Compd*, 583 (2014) 320.
16 Farhadi S, Momeni Z & Taherimehr M, *J Alloys Compd*, 471 (2009) L5.
17 Kumar M, Srikanth S, Ravikumar B, Alex T C & Das S K, *Mater Chem Phys*, 113 (2009) 803.
18 Gosavi P V & Biniwale R B, *Mater Chem Phys*, 119 (2010) 324.
19 Yang Z, Huang Y, Dong B & Li H L, *Mater Res Bull*, 41 (2006) 274.
20 Chung S H, Chiu K C & Jean J H, *Jpn J Appl Phys*, 47 (2008) 8498.
21 Liu T & Xu Y, *Mater Chem Phys*, 129 (2011) 1047.
22 Shen H, Cheng G, Wu A, Xu J & Zhao, J *Phys Status Solidi A*, 206 (2009) 1420.
23 Qi X, Zhou J, Yue Z, Gui Z & Li L, *Mater Chem Phys*, 78 (2002) 25.
24 Jain S R, Adiga K C & Verneker V R P, *Combust Flame*, 40 (1981) 71.
25 Singh S & Singh D, *Monatsh Chem*, (2016) doi: 10.1007/s00706-016-1818-3.

26 Phadatare M R, Salunkhe A B, Khot V M, Sathish C I, Dhawale D S & Pawar S H, *J Alloys Compd*, 546 (2013) 314.

27 Larson A C & Von Dreele R B, *General Structure Analysis System* (*GSAS*), (Los Alamos National Laboratory Report LAUR) 2004, p. 86.

28 Klug H P & Alexander L E, *X-ray Diffraction Procedures for Polycrystalline and Amorphous Materials*, (Wiley, New York) 1997, p. 637.

29 Conceição L, Silva A M, Ribeiro N F P & Souza M M V M, *Mater Res Bull*, 46 (2011) 308.

30 Conceição L, Ribeiro N F P, Furtado J G M & Souza M M V M, *Ceram Int*, 35 (2009) 1683.

31 Cullity B D, *Elements of X-ray Diffraction Reading*, 2nd Edn, (Addison-Wesley Publishing Co, USA).

32 Hwang C-C, Tsai J-S, Huang T-H, Peng C-H & Chen S-Y, *J Solid State Chem*, 178 (2005) 382.

33 Siwach P K, Goutam U K, Srivastava P, Singh H K, Tiwari R S & Srivastava O N, *J Phys D Appl Phys*, 39 (2006) 14.

34 Nica V, Sauer H M, Embs J & Hempelmann R, *J Phys Condens Matter*, 20 (2008) 204115.

35 Georgea M, Johna A M, Naira S S, Joyb P A & Anantharamana M R , *J Magn Magn Mat*, 302 (2006) 190.

36 Fita I, Markovich V, Mogiyansky D, Puzniak R, Wisniewski A, Titelman L, Vradman L, Herskowitz M, Varyukhin V N & Gorodetsky G, *Phys Rev B*, 77 (2008) 224421.

37 Singh D, Choudhary N, Mahajan A, Singh S & Sharma S, *Ionics*, 21 (2015) 1031.

38 Goodenough J B, *Magnetism and the Chemical Bond*, (Interscience, New York) 1963.

39 Kanamori J, *J Phys Chem Solids*, 10 (1959) 87.

40 Gupta S, Verma M K & Singh D, *Ceram Int*, 42 (2016) 18418.

1048